Sound radiation from a semi-infinite lined duct

N. Peake[a], I.D. Abrahams[b]

[a] *Department of Applied Mathematics and Theoretical Physics, University of Cambridge, Wilberforce Road, Cambridge CB3 0WA UK*
[b] *Issac Newton Institute for Mathematical Sciences, 20 Clarkson Road, Cambridge CB3 0EH UK*

Abstract

In this paper we consider the radiation properties of a pair of semi-infinite, parallel-plate ducts in which the inner duct is buried inside the outer duct. A Robin condition is applied to one of the inner walls (to represent an acoustic lining), while Neumann conditions are applied on all other surfaces. This leads to a matrix Wiener-Hopf problem, which requires the factorisation of a 3×3 matrix of a form which, to our knowledge, has not previously been considered in the literature and which is not directly amenable to standard pole-removal techniques. We derive the exact factorisation of this matrix here, and present results for the far-field scattered sound which show the effect of varying the properties of the wall lining.

Keywords: Sound, ducts, acoustic lining, Wiener-Hopf technique

1. Introduction

Calculation of the sound emitted from the open end of a duct is a classical problem in wave scattering, and has received considerable attention. In early work, Lord Rayleigh [1] considered a circular cylindrical duct and calculated the reflected amplitude and end correction for a plane wave under the approximation that the open end is flanged, while Levine & Schwinger calculated an exact solution for an unflanged cylinder [2], and Homicz & Lordi [3] presented results for the far-field radiation pattern produced by asymmetric duct modes. The two-dimensional analogue of ducts formed by parallel plates has also been much studied, and full details of the classical solutions in both geometries are given in [4]. Extensions have been made in several directions, often inspired by specific practical applications; for instance, Munt [5, 6] considered the problem of the sound from a jet issuing from a cylindrical pipe, as a model of rearward noise radiation from aeroengines. Gabard & Astley [7] extended Munt's model to include an infinite centre-body, as a partial model of the engine jet pipe. In a different direction, Rawlins [8] considered a semi-infinite cylindrical duct enclosed concentrically within an infinite duct, as a model of a car exhaust muffler.

The problems referred to in the previous paragraph can be completed by application of the so-called scalar Wiener-Hopf technique [9]. Here one must determine two unknowns functions from a single Wiener-Hopf equation, and this requires, inter alia, the multiplicative factorisation of a scalar function $f(\alpha)$ in the form $f(\alpha) = f^+(\alpha)f^-(\alpha)$, with $f^\pm(\alpha)$ being analytic, nonzero and with algebraic behaviour at infinity in the upper and lower halves of the complex α (Fourier) plane respectively. However, more complicated problems often lead to matrix Wiener-Hopf systems, and we mention specifically here the work of Veitch & Peake [10], who considered sound radiation from the exhaust flow of rigid coaxial cylinders in which the duct terminations are not necessarily coplanar. Here four unknown functions must be found from two Wiener-Hopf equations, and this requires the factorisation of a 2×2 matrix $\boldsymbol{\mathcal{K}}(\alpha)$ in the form $\boldsymbol{\mathcal{K}}^-(\alpha)\boldsymbol{\mathcal{K}}(\alpha) = \boldsymbol{\mathcal{K}}^+(\alpha)$ with $\boldsymbol{\mathcal{K}}^\pm(\alpha)$ being analytic, invertible and with algebraic behaviour at infinity in the respective half planes. Unlike for scalar problems no general method exists for completing this matrix factorisation, and classes of problems must be solved on a case by case basis - for instance, in [10], different solution methods are required when the inner cylinder is buried inside or protrudes beyond the outer cylinder.

The papers referred to above consider rigid duct walls (Neumann boundary conditions), but acoustic linings are often used in aeroengines and can be represented using impedance (Robin) boundary conditions [11]. The Munt solution [5] has been extended in this way by Rawlins [12], while Demir & Rienstra [13, 14] solved the problem of sound emission by a semi-infinite outer cylinder containing an infinite centre-body which is lined downstream of the open end and is rigid upstream. It is clear from these papers that replacement of a Neumann by a Robin boundary condition complicates the problems, since one is moving from a situation in which one unsteady variable is known exactly on the wall to a situation in which two unsteady variables are related to one another on the wall but are otherwise unknown. In this paper our aim is therefore to work towards extending the work of Veitch & Peake [10] to allow for a wall lining, and since the modification of the wall condition appears to be the most significant step we will restrict our attention here to the case of a parallel-plate duct in which the inner-duct termination is buried. As we will see, this will require factorisation of a 3×3 Wiener-Hopf matrix $\boldsymbol{\mathcal{K}}$ (compared to 2×2 matrix in the rigid-wall case), and therefore involves additional complexity. In particular, we believe that $\boldsymbol{\mathcal{K}}$ is of a form not previously treated in the literature.

This paper is set out as follows: the problem formulation and formal Wiener-Hopf solution are presented in section 2; the factorisation of the 3×3 matrix $\boldsymbol{\mathcal{K}}$ is described in section 3 in terms of a 2×2 submatrix $\boldsymbol{\mathcal{L}}$, which itself is factorised in section 4; numerical results and concluding remarks are presented in sections 5 and 6; and the final results of the matrix factorisation and, for comparison, the rigid wall solution, are given in appendices.

2. Problem Formulation and formal solution

We consider the two-dimensional model of acoustic radiation from a semi-infinite duct with walls lying along $x < 0$, $y = \pm 1$, and which contains a second semi-infinite duct with walls $x < d, y = \pm a$; note that $a < 1$ and all lengths have been nondimensionalised by scaling on the half-width of the outer duct. We take $d \leqslant 0$, so that the inner duct is either buried a finite distance inside the outer duct, or, if $d = 0$, the duct terminations are coplanar. All the surfaces are rigid, apart from the outer surfaces of the inner duct walls, which will be compliant, see Figure 1.

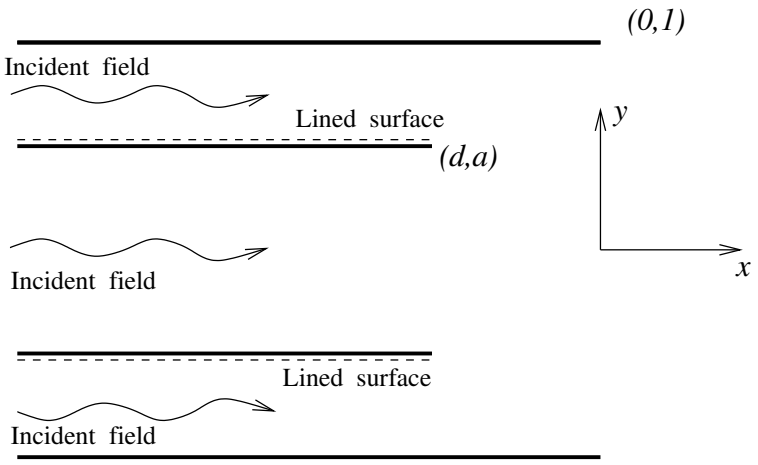

Figure 1: The model problem. The system is symmetric about $y = 0$.

An incident sound wave of nondimensional radian frequency ω propagates in either the outer or inner duct (here time has been made nondimensional using the uniform undisturbed sound speed and the outer duct half-width, so that ω is the Helmholtz number with respect to the outer duct). We will consider the velocity potential of the total unsteady field, $\mathrm{Re}\,\{\phi_t(x,y)\exp(-\mathrm{i}\omega t)\}$, where $\mathrm{Re}\{\ldots\}$ denotes the real part, and in what follows the factor $\exp(-\mathrm{i}\omega t)$ will be suppressed for brevity. The total field is made up of the incident field plus the unknown field scattered from the duct terminations, so that

$$\phi_t = \begin{cases} \phi & |y| \geqslant 1\ , \\ \phi + \phi_{\mathrm{inc}} & a \leqslant |y| \leqslant 1\ , \\ \phi + \phi_{\mathrm{inc}} & 0 \leqslant |y| \leqslant a\ . \end{cases} \tag{1}$$

Note that the incident field is taken to consist of incident waves from $x = -\infty$ in the region between the respective pairs of plates (i.e. in the outer ducts), as well as incident waves from $x = -\infty$ in the region between the inner plates. The potentials satisfy the Helmholtz equation

$$\boldsymbol{\nabla}^2\phi + \omega^2\phi = 0\ , \tag{2}$$

with the following boundary conditions in $y \geqslant 0$ (and in $y \leqslant 0$ symmetrically):

(a) zero total normal velocity on both sides of the walls $y = 1, x < 0$, and on $y = a-, x < d$;

(b) on the outer face of the inner wall , $y = a+, x < d$, the Robin condition

$$\delta\phi + \beta\frac{\partial\phi}{\partial y} = 0 \,, \tag{3}$$

holds, with β, δ given complex constants;

(c) the total unsteady pressure (and therefore ϕ_t) is continuous throughout the fluid, and in particular across $y = 1, x > 0$ and $y = a, x > d$, and is bounded everywhere;

(d) the incident field is taken to be symmetric in y, so that the scattered field satisfies $\partial\phi/\partial y = 0$ on $y = 0$ for all x;

(e) the field is outgoing or decaying as $r = \sqrt{x^2 + y^2} \to \infty$.

By considering the wall boundary conditions in the outer duct for all x it is straightforward to show that the field in $a \leqslant |y| \leqslant 1$, $x < d$ is composed purely of modes with axial wavenumbers $\mu_n^{\pm}$, say, for $n = 0, 1, 2, ...$, where the superscripts $^{\pm}$ indicate modes in the upper/lower halves of the complex plane which, in general, propagate or decay in the negative/positive x directions respectively. (For pure propagation without decay, a mode $\mu_n^{\pm}$ must have zero imaginary part.) The $\mu_n^{\pm}$ will be shown to be the roots of the dispersion relation

$$\Delta(\alpha) \equiv \delta\cosh[\gamma(\alpha)(1-a)] - \beta\gamma(\alpha)\sinh[\gamma(\alpha)(1-a)] = 0 \,, \tag{4}$$

where

$$\gamma(\alpha) = \sqrt{\alpha^2 - \omega^2} \,, \tag{5}$$

with branch cuts joining the branch points $\pm\omega$ to infinity through the upper and lower half planes respectively, and with $\gamma(\alpha)$ defined to be real and positive as α approaches infinity along the positive (and negative) real axis. Similarly, in $|y| \leqslant a$, $x < d$ the field is composed purely of modes with axial wavenumbers $\kappa_n^{\pm}$, say, for $n = 0, 1, 2, ...$, which satisfy the simple rigid-duct dispersion relation

$$\sinh[\gamma(\alpha)] = 0 \,. \tag{6}$$

The incident potential, corresponding to a single such mode in each region, is of the form

$$\phi_{\rm inc} = \begin{cases} K\cosh[\gamma(\mu_{\rm inc})(1-y)]\exp(-{\rm i}\mu_{\rm inc}x) & a \leqslant |y| \leqslant 1 \,, \\ J\cos[M\pi y/a]\exp(-{\rm i}\kappa_{inc}x) & 0 \leqslant |y| \leqslant a \,, \end{cases} \tag{7}$$

where $\mu_{\rm inc}$ is one of the modes μ_n^- and $\kappa_{\rm inc}$ is one of the modes κ_n^- ($\kappa_{\rm inc} = \kappa_M^-$ for definiteness). In section 5 we will consider separately scattering of incident modes in the outer and inner ducts, by setting the normalisation constants J, K to zero respectively, while choosing K, J respectively so as to enforce unit incident power flux across the termination $x = d$. It should be noted that the

fact that modes which propagate (and possible decay) in the positive x direction possess complex wavenumbers which lie in the lower half of the complex α is a direct consequence of our choices of $\exp(-\mathrm{i}\omega t)$ time dependence and the Fourier transform convention stated in the next paragraph.

In order to determine the scattered field we introduce the full-range axial Fourier transform

$$\Phi(\alpha, y) = \int_{-\infty}^{\infty} \phi(x, y) \exp(\mathrm{i}\alpha x) \mathrm{d}x \ , \tag{8}$$

and transforming (2) we find that

$$\Phi(\alpha, y) = \begin{cases} A\cosh(\gamma y), & y \leqslant a \ , \\ B\cosh(\gamma y) + C\sinh(\gamma y), & a \leqslant y \leqslant 1 \ , \\ D\exp(-\gamma y), & y \geqslant 1 \ , \end{cases} \tag{9}$$

where A, B, C, D are as yet unknown functions of α. Note that the form of the top and bottom elements of (9) ensures satisfaction of boundary conditions (d) and (e) respectively. We now proceed to apply the remaining boundary conditions (a-c). After some algebra we find the vector equation

$$\boldsymbol{\Psi}^- = \boldsymbol{\mathcal{K}} \boldsymbol{\Upsilon}^+ + \frac{\boldsymbol{F}}{\alpha - \mu_{\mathrm{inc}}} + \frac{\boldsymbol{G}}{\alpha - \kappa_{\mathrm{inc}}} \ , \tag{10}$$

where the vector $\boldsymbol{\Upsilon}^+$ is given by

$$\boldsymbol{\Upsilon}^+ = \left(\frac{\partial \Phi^+}{\partial y}(\alpha, 1), \tilde{\Phi}^+(\alpha, a), \frac{\partial \Phi^+}{\partial y}(\alpha, a) \right)^T \ . \tag{11}$$

The superscript $^+$ denotes that the Fourier transforms in this expression have been taken only over the portions of the x axis downstream of the trailing edges, so that the first element of the vector in (11) is the half-range Fourier transform of the scattered normal velocity on $y = 1, x > 0$ and $[\partial \Phi^+ / \partial y](\alpha, a) \exp(\mathrm{i}\alpha d)$ is the half-range transform of the scattered normal velocity on $y = 1, x > d$. The factor $\exp(\mathrm{i}\alpha d)$ is introduced into the definition of the second half-range transform in order to ensure algebraic growth at infinity of the function $[\partial \Phi^+ / \partial y](\alpha, a)$. The second component in (11) is

$$\tilde{\Phi}^+(\alpha, a) = \left[\delta \Phi^+(\alpha, a) + \beta \frac{\partial \Phi^+}{\partial y}(\alpha, a) \right] \ , \tag{12}$$

which, when multiplied by $\exp(\mathrm{i}\alpha d)$, corresponds to the half range Fourier transform of the quantity on the left of (3) over $y = a, x > d$. From the theory of half-range Fourier transforms [9], all quantities with the superscript $^+$ are analytic (and of algebraic growth) in the upper half of the complex α plane, which here includes the positive real line. The vector $\boldsymbol{\Psi}^-$ in (10) is given by

$$\boldsymbol{\Psi}^- = \left(\left\{ \Phi^-(\alpha, 1-) - \Phi^-(\alpha, 1+) \right\}, \left\{ \Phi^-(\alpha, a+) - \Phi^-(\alpha, a-) \right\}, \frac{\partial \Phi^-}{\partial y}(\alpha, a+) \right) \ , \tag{13}$$

where the first two terms are simply the half-range Fourier transforms of the jumps in the scattered potentials across the walls $y = 1, x < 0$ and $y = a, x < d$ respectively, and the third component is related to the transform of the wall-normal velocity on $y = a+$ over $x < d$. As above, the latter two half-range Fourier transforms have been scaled on $\exp(\mathrm{i}\alpha d)$ to ensure algebraic growth at infinity, and all quantities with the superscript $^-$ are analytic in the lower half of the complex α plane including the negative real line. The 3×3 matrix $\boldsymbol{\mathcal{K}}$ in (10) is

$$\boldsymbol{\mathcal{K}} = \begin{pmatrix} \left[\frac{\delta-\beta\gamma}{\gamma\Delta}\right] e^{(1-a)\gamma} & \frac{e^{\mathrm{i}\alpha d}}{\Delta} & 0 \\ -\frac{\beta e^{-\mathrm{i}\alpha d}}{\Delta} & \frac{\cosh(\gamma(1-a))}{\Delta} & -\frac{\cosh(\gamma a)}{\gamma \sinh(\gamma a)} \\ \frac{\delta e^{-\mathrm{i}\alpha d}}{\Delta} & -\frac{\gamma \sinh(\gamma(1-a))}{\Delta} & -1 \end{pmatrix} , \tag{14}$$

where $\Delta(\alpha)$ is given in (4). Finally, the constant vectors $\boldsymbol{F}, \boldsymbol{G}$ in (10) are given by

$$\begin{aligned} \boldsymbol{F} &= \left(\mathrm{i}K, \mathrm{i}K\cosh[\gamma(\mu_{\mathrm{inc}})(1-a)]e^{-\mathrm{i}\mu_{\mathrm{inc}}d}, -\mathrm{i}K(\delta/\beta)\cosh[\gamma(\mu_{\mathrm{inc}})(1-a)]e^{-\mathrm{i}\mu_{\mathrm{inc}}d}\right)^T \\ \boldsymbol{G} &= \left(0, -\mathrm{i}J\cos[M\pi]e^{-\mathrm{i}\kappa_{\mathrm{inc}}d}, 0\right)^T , \end{aligned} \tag{15}$$

and arise due to the presence of the incident field.

We now wish to factorise the matrix $\boldsymbol{\mathcal{K}}$ in the form

$$\boldsymbol{\mathcal{K}}^-\boldsymbol{\mathcal{K}} = \boldsymbol{\mathcal{K}}^+ , \tag{16}$$

where the matrices $\boldsymbol{\mathcal{K}}^\pm$ are analytic, invertible and have algebraic behaviour at infinity in the upper and lower half α planes respectively. The method for completing this factorisation will be described in the next section. Once it has been completed, we can then rearrange (10) to obtain the vectorial Wiener-Hopf equation

$$\begin{aligned} \boldsymbol{\mathcal{K}}^+(\alpha)\boldsymbol{\Upsilon}^+ + \frac{\boldsymbol{\mathcal{K}}^-(\mu_{\mathrm{inc}})\boldsymbol{F}}{\alpha-\mu_{\mathrm{inc}}} + \frac{\boldsymbol{\mathcal{K}}^-(\kappa_{\mathrm{inc}})\boldsymbol{G}}{\alpha-\kappa_{\mathrm{inc}}} \\ = \boldsymbol{\mathcal{K}}^-\boldsymbol{\Psi}^- - \frac{[\boldsymbol{\mathcal{K}}^-(\alpha)-\boldsymbol{\mathcal{K}}^-(\mu_{\mathrm{inc}})]\boldsymbol{F}}{\alpha-\mu_{\mathrm{inc}}} - \frac{[\boldsymbol{\mathcal{K}}^-(\alpha)-\boldsymbol{\mathcal{K}}^-(\kappa_{\mathrm{inc}})]\boldsymbol{G}}{\alpha-\kappa_{\mathrm{inc}}} . \end{aligned} \tag{17}$$

In this form the left hand side is analytic in the upper half of the complex α plane and the right hand side is analytic in the lower half plane, so that by analytic continuation we can define an entire (vector) function, $\boldsymbol{E}(\alpha)$ say. In order to find the solution which is least singular at the plate edges we set $\boldsymbol{E}(\alpha) \equiv \boldsymbol{0}$, so that both sides of (17) are identically zero. (This result can be confirmed *a posteriori*.) This leaves us with two equations, from which we can determine the two unknown vectors $\boldsymbol{\Upsilon}^+$ & $\boldsymbol{\Psi}^-$ and hence A, B, C and D. The solution of the problem is therefore obtained. In section 5 we will show results for the far-field sound ($y \to \infty$), and hence we need give only the expression for the previously unknown quantity D as

$$D(\alpha) = \frac{e^\gamma}{\gamma}\left\{\frac{[\boldsymbol{\mathcal{K}}^+(\alpha)]^{-1}\boldsymbol{\mathcal{K}}^-(\mu_{\mathrm{inc}})\boldsymbol{F}}{\alpha-\mu_{\mathrm{inc}}} + \frac{[\boldsymbol{\mathcal{K}}^+(\alpha)]^{-1}\boldsymbol{\mathcal{K}}^-(\kappa_{\mathrm{inc}})\boldsymbol{G}}{\alpha-\kappa_{\mathrm{inc}}}\right\}_1 , \tag{18}$$

where the subscript $_1$ indicates the first component of the vector is to be taken.

3. Factorisation of the 3×3 matrix $\boldsymbol{\mathcal{K}}$

The key step in determining the solution (18) above is the factorisation (16). As mentioned in the introduction, matrix kernel factorisation is in general a difficult exercise, but specific classes of matrices exist which permit explicit decomposition. Here, with $d < 0$, we expect to be able to obtain $\boldsymbol{\mathcal{K}}^{\pm}$ via the pole removal technique (see e.g. [15]). However, the form of (14) is such that it does not appear to fit any of the classes already examined in the literature. Thus, its decomposition offers a novel approach to the theory of matrix factorisation.

In order to calculate the elements $k_{ij}^{\pm}(\alpha)$ of $\boldsymbol{\mathcal{K}}^{\pm}$ we start by considering the i-2 and i-3 elements in (16) for $i = 1, 2, 3$, which we combine as

$$\begin{pmatrix} e^{\mathrm{i}\alpha d}/\Delta \\ 0 \end{pmatrix} k_{i1}^{-} - \begin{pmatrix} k_{i2}^{+} \\ k_{i3}^{+} \end{pmatrix} = \boldsymbol{\mathcal{L}} \begin{pmatrix} k_{i2}^{-} \\ k_{i3}^{-} \end{pmatrix} , \tag{19}$$

where the 2×2 matrix $\boldsymbol{\mathcal{L}}$ is given by

$$\boldsymbol{\mathcal{L}} = \begin{pmatrix} -\frac{\cosh(\gamma(1-a))}{\Delta} & \frac{\gamma \sinh(\gamma(1-a))}{\Delta} \\ \frac{\cosh(\gamma a)}{\gamma \sinh(\gamma a)} & 1 \end{pmatrix} . \tag{20}$$

The remaining i-1 column in (16) can, by using (19) to eliminate $k_{i2,3}^{-}$ and after some manipulation, be re-expressed as

$$\frac{k_{i1}^{-}(\alpha)}{q(\alpha)} = e^{-\mathrm{i}\alpha d} \left(\left[\frac{\delta \cosh(\gamma a) + \beta\gamma \sinh(\gamma a)}{\gamma \sinh\gamma} \right] k_{i2}^{+}(\alpha) + \left[\frac{\sinh(\gamma a)}{\sinh\gamma} \right] k_{i3}^{+}(\alpha) \right) + k_{i1}^{+}(\alpha) , \tag{21}$$

where

$$q(\alpha) \equiv \gamma e^{-\gamma} \sinh\gamma . \tag{22}$$

The reason for writing the matrix factorization in the dual form, (19) and (21), and the key to obtaining the decomposition matrices $\boldsymbol{\mathcal{K}}^{\pm}$ is that the exponential factors $e^{i\alpha d}$, and $e^{-i\alpha d}$, appear explicitly as multiplicative factors of the unknown functions k_{i1}^{-}, and k_{i2}^{+} and k_{i3}^{+}, respectively. As $d < 0$ these exponential terms decay in the respective half planes of analyticity of the factors that they multiply and, as will be shown, permit an efficient solution technique to be applied. Note that, for $d > 0$, i.e. when the inner duct protrudes from the outer duct, the following approach cannot be applied.

To solve (21) we make the scalar multiplicative factorisation of $q(\alpha)$ in the form $q(\alpha) = q^{+}(\alpha) q^{-}(\alpha)$ given in (B.3), with $q^{\pm}(\alpha)$ analytic, nonzero and with algebraic behaviour at infinity in the upper/lower halves of the complex α plane respectively. After multiplying (21) through by $q^{+}(\alpha)$, poles are still present at $\alpha = \alpha_n^{\pm}$ for $n = 0, 1, 2, ...$, corresponding to the zeros of $\gamma \sinh\gamma$ in the upper/lower halves of the α plane. It is easy to show that

$$\alpha_n^{\pm} = \begin{cases} \pm\sqrt{\omega^2 - n^2\pi^2} & \text{if } \omega > n\pi , \\ \pm\mathrm{i}\sqrt{n^2\pi^2 - \omega^2} & \text{if } \omega < n\pi . \end{cases} \tag{23}$$

The pole removal method [15] can now be employed to eliminate poles at $\alpha = \alpha_n^+$ from the right hand side of (21), and arrive at the Wiener-Hopf equation

$$\frac{k_{i1}^-(\alpha)}{q^-(\alpha)} - \sum_{n=0}^{\infty} \frac{q^+(\alpha_n^+)}{\alpha - \alpha_n^+} e^{-\mathrm{i}\alpha_n^+ d} \left[R_n^1 k_{i2}^+(\alpha_n^+) + R_n^2 k_{i3}^+(\alpha_n^+)\right] =$$
$$q^+(\alpha) e^{-\mathrm{i}\alpha d} \left(\left[\frac{\delta \cosh(\gamma a) + \beta\gamma \sinh(\gamma a)}{\gamma \sinh\gamma} \right] k_{i2}^+(\alpha) + \left[\frac{\sinh(\gamma a)}{\sinh\gamma} \right] k_{i3}^+(\alpha) \right)$$
$$- \sum_{n=0}^{\infty} \frac{q^+(\alpha_n^+)}{\alpha - \alpha_n^+} e^{-\mathrm{i}\alpha_n^+ d} \left[R_n^1 k_{i2}^+(\alpha_n^+) + R_n^2 k_{i3}^+(\alpha_n^+)\right] + q^+(\alpha) k_{i1}^+(\alpha) \, . \qquad (24)$$

Here

$$R_n^1 = \epsilon_n (-1)^n (\delta \cos(n\pi a) - \beta n\pi \sin(n\pi a))/\alpha_n^+, \qquad (25)$$
$$R_n^2 = -(-1)^n n\pi \sin(n\pi a)/\alpha_n^+ \qquad (26)$$

are the corresponding residues, with $\epsilon_0 = 1/2$ and $\epsilon_n = 1$ otherwise. We now note that the left/right hand sides of (24) are analytic in the lower/upper half planes, thereby defining by analytic continuation an entire function. Without loss of generality, we can take this entire function to be a constant, C_i for $i = 1, 2, 3$, and this leads to expressions for $k_{i1}^{\pm}(\alpha)$ (see equations A.1, A.3).

Returning to equation (19) we now suppose that the 2×2 matrix $\boldsymbol{\mathcal{L}}(\alpha)$ can be factorised in the form

$$\boldsymbol{\mathcal{L}}^+ \boldsymbol{\mathcal{L}} = \boldsymbol{\mathcal{L}}^- \, , \qquad (27)$$

where the matrices $\boldsymbol{\mathcal{L}}^{\pm}$ are analytic, invertible and have algebraic behaviour at infinity in the upper and lower half α planes respectively. The method for completing this factorisation will be described in the next section. We now multiply (19) by $\boldsymbol{\mathcal{L}}^+$, and after some rearrangement find that

$$\boldsymbol{\mathcal{L}}^-(\alpha) \begin{pmatrix} k_{i2}^-(\alpha) \\ k_{i3}^-(\alpha) \end{pmatrix} + e^{\mathrm{i}\alpha d} k_{i1}^-(\alpha) \boldsymbol{\mathcal{L}}^-(\alpha) \begin{pmatrix} \sinh(\gamma a)/\sinh\gamma \\ -\cosh(\gamma a)/\gamma\sinh\gamma \end{pmatrix}$$
$$+ \sum_{n=0}^{\infty} \frac{k_{il}^-(\alpha_n^-)}{\alpha - \alpha_n^-} e^{\mathrm{i}\alpha_n^- d} \boldsymbol{\mathcal{L}}^-(\alpha_n^-) \begin{pmatrix} S_n^1 \\ S_n^2 \end{pmatrix} =$$
$$-\boldsymbol{\mathcal{L}}^+(\alpha) \begin{pmatrix} k_{i2}^+(\alpha) \\ k_{i3}^+(\alpha) \end{pmatrix} + \sum_{n=0}^{\infty} \frac{k_{il}^-(\alpha_n^-)}{\alpha - \alpha_n^-} e^{\mathrm{i}\alpha_n^- d} \boldsymbol{\mathcal{L}}^-(\alpha_n^-) \begin{pmatrix} S_n^1 \\ S_n^2 \end{pmatrix} \, . \qquad (28)$$

Here we have again used the pole removal method on the zeros α_n^- of $\gamma\sinh\gamma$ in the lower half plane, and

$$S_n^1 = (-1)^n n\pi \sin(n\pi a)/\alpha_n^- , \qquad S_n^2 = \epsilon_n (-1)^n \cos(n\pi a)/\alpha_n^- \qquad (29)$$

are the corresponding residues. Now note that the left/right hand sides of (28) are analytic in the lower/upper halves of the complex plane respectively, so by analytic continuation we have a 2-vector with entire components, which we can

set to be constant, $\tilde{\boldsymbol{C}}_i$ say for $i = 1, 2, 3$. This leads to expressions for $k^{\pm}_{i2,3}(\alpha)$ (see equations A.2, A.4).

So far we have only determined the factors of $\boldsymbol{\mathcal{K}}(\alpha)$ implicitly in terms of the unknown quantities $k^{-}_{i1}(\alpha^{-}_n)$ and $k^{+}_{i2,3}(\alpha^{+}_n)$ for $n = 0, 1, \ldots$. In order to complete the factorisation in closed form we now set $\alpha = \alpha^{-}_p$ in (A.3) and $\alpha = \alpha^{+}_n$ in (A.2), allowing us to form the infinite set of algebraic equations

$$[\boldsymbol{\mathcal{I}} - \boldsymbol{\mathcal{A}}]\, \boldsymbol{k} = \boldsymbol{v} \;, \tag{30}$$

where

$$\begin{aligned}
\mathcal{A}_{pm} &= q^{-}(\alpha^{-}_p) \sum_{n=0}^{\infty} \frac{q^{+}(\alpha^{+}_n) e^{-\mathrm{i}(\alpha^{+}_n - \alpha^{-}_m)d}}{(\alpha^{-}_p - \alpha^{+}_n)(\alpha^{+}_n - \alpha^{-}_m)} \begin{pmatrix} R^1_n & R^2_n \end{pmatrix} \left[\boldsymbol{\mathcal{L}}^{+}(\alpha^{+}_n)\right]^{-1} \boldsymbol{\mathcal{L}}^{-}(\alpha^{-}_m) \begin{pmatrix} S^1_m \\ S^2_m \end{pmatrix}, \\
v_p &= q^{-}(\alpha^{-}_p) \left[C_i - \sum_{n=0}^{\infty} \frac{q^{+}(\alpha^{+}_n) e^{-\mathrm{i}\alpha_n d}}{\alpha^{-}_p - \alpha^{+}_n} \begin{pmatrix} R^1_n & R^2_n \end{pmatrix} \left[\boldsymbol{\mathcal{L}}^{+}(\alpha^{+}_n)\right]^{-1} \tilde{\boldsymbol{\mathcal{C}}}_i \right], \\
k_p &= k^{-}_{i1}(\alpha^{-}_p) \;,
\end{aligned} \tag{31}$$

and $\boldsymbol{\mathcal{I}}$ is the identity matrix. Equation (30) can now be truncated to finite order and solved numerically to give the unknown $k^{-}_{i1}(\alpha^{-}_p)$. (Specifically, the first iterate of (30) was truncated, and the size of the truncation increased until converged results were obtained.) The unknowns $k^{+}_{i2,3}(\alpha^{+}_n)$ can then be found from (A.2). Putting all this together we have therefore found expressions for the factors of $\boldsymbol{\mathcal{K}}(\alpha)$ in terms of the factors of the 2×2 submatrix $\boldsymbol{\mathcal{L}}$. The factorisation of $\boldsymbol{\mathcal{L}}$ will be described in the next section.

4. Factorisation of the 2×2 matrix $\boldsymbol{\mathcal{L}}$

We start by equating the i-1 elements in (27), which after rearrangement gives

$$Q(\alpha) \left[-\frac{\cosh(\gamma(1-a))\sinh(\gamma a)}{\sinh\gamma} l^{+}_{i1} + \frac{\Delta\cosh(\gamma a)}{\gamma\sinh\gamma} l^{+}_{i2} \right] = l^{-}_{i1} \;, \tag{32}$$

where $l^{\pm}_{ij}$ are the elements of $\boldsymbol{\mathcal{L}}^{\pm}$,

$$Q(\alpha) = \frac{\sinh\gamma}{\Delta\sinh(\gamma a)} \;, \tag{33}$$

and $\Delta(\alpha)$ is given in (4). In due course we will require the scalar multiplicative factorisation of $Q(\alpha)$ in the form $Q(\alpha) = Q^{+}(\alpha)Q^{-}(\alpha)$, with $Q^{\pm}(\alpha)$ analytic, nonzero and with algebraic behaviour at infinity in the upper/lower halves of the complex α plane respectively. Similarly, equating the i-2 elements in (27) gives

$$l^{+}_{i1} \frac{\gamma\sinh(\gamma(1-a))}{\Delta} + l^{+}_{i2} = l^{-}_{i2} \;. \tag{34}$$

We now proceed by using the pole removal method. Specifically, we subtract the residues of the poles corresponding to the zeros of $\gamma\sinh\gamma$ in the upper half plane, namely α_n^+, from (32) and to the zeros of Δ in the upper half plane, μ_n^+, from (34). These equations can then be rearranged into the usual Wiener-Hopf form, from which it becomes clear that $\boldsymbol{\mathcal{L}}^-(\alpha)$ takes the generic form

$$\boldsymbol{\mathcal{L}}^-(\alpha) = \begin{pmatrix} Q^-(\alpha)\left[1+\sum_{m=0}^{\infty}\frac{a_m^{(1)}}{\alpha-\alpha_m^+}\right] & \sum_{m=0}^{\infty}\frac{b_m^{(1)}}{\alpha-\mu_m^+} \\ Q^-(\alpha)\sum_{m=0}^{\infty}\frac{a_m^{(2)}}{\alpha-\alpha_m^+} & 1+\sum_{m=0}^{\infty}\frac{b_m^{(2)}}{\alpha-\mu_m^+} \end{pmatrix}, \tag{35}$$

where the constants $a_m^{(1,2)}, b_m^{(1,2)}$ are at this stage unknown. From (27) it follows that the elements of $\boldsymbol{\mathcal{L}}^+(\alpha)$ are of the form

$$\begin{aligned}
l_{11}^+ &= -\frac{1}{Q^+(\alpha)}\left[1+\sum_{m=0}^{\infty}\frac{a_m^{(1)}}{\alpha-\alpha_m^+}\right] + \frac{\Delta\cosh(\gamma a)}{\gamma\sinh\gamma}\sum_{m=0}^{\infty}\frac{b_m^{(1)}}{\alpha-\mu_m^+}, \\
l_{21}^+ &= -\frac{1}{Q^+(\alpha)}\left[\sum_{m=0}^{\infty}\frac{a_m^{(2)}}{\alpha-\alpha_m^+}\right] + \frac{\Delta\cosh(\gamma a)}{\gamma\sinh\gamma}\left[1+\sum_{m=0}^{\infty}\frac{b_m^{(2)}}{\alpha-\mu_m^+}\right], \\
l_{12}^+ &= \frac{\gamma\sinh(\gamma(1-a))}{\Delta Q^+(\alpha)}\left[1+\sum_{m=0}^{\infty}\frac{a_m^{(1)}}{\alpha-\alpha_m^+}\right] + \frac{\cosh(\gamma(1-a))\sinh(\gamma a)}{\sinh\gamma}\sum_{m=0}^{\infty}\frac{b_m^{(1)}}{\alpha-\mu_m^+}, \\
l_{22}^+ &= \frac{\gamma\sinh(\gamma(1-a))}{\Delta Q^+(\alpha)}\left[\sum_{m=0}^{\infty}\frac{a_m^{(2)}}{\alpha-\alpha_m^+}\right] + \frac{\cosh(\gamma(1-a))\sinh(\gamma a)}{\sinh\gamma}\left[1+\sum_{m=0}^{\infty}\frac{b_m^{(2)}}{\alpha-\mu_m^+}\right].
\end{aligned} \tag{36}$$

Note that the expression for the minus factor in (35) can be seen to be analytic in the lower half plane, but the elements of the plus factor in (36) apparently have poles at each $\alpha = \alpha_m^+, \mu_m^+$ for $m = 0, 1, 2, ...$ Thus, we must select the values of the constants $a_m^{(1,2)}, b_m^{(1,2)}$ in order to remove these singularities, and thereby render (36) analytic in the upper half plane as required.

Taking l_{11}^+ in (36) first, it appears to have poles in the upper half plane at $\alpha = \alpha_m^+$ for $m = 0, 1, 2....$ To remove these we require the residues to be zero, and so

$$a_n^{(1)} = \left[\epsilon_n Q^+(\alpha_n^+)\Delta(\alpha_n^+)(-1)^n\cos(n\pi a)/\alpha_n^+\right]\sum_{m=0}^{\infty}\frac{b_m^{(1)}}{\alpha_n^+-\mu_m^+}, \tag{37}$$

where as before $\epsilon_0 = 1/2$ and $\epsilon_n = 1$, $n > 0$. With this condition l_{11}^+ is analytic in the upper half plane as the apparent poles at $\alpha = \mu_m^+$ are cancelled by the zeros of $\Delta(\alpha)$. Similarly, by requiring the residues of the apparent poles in l_{12}^+ at all $\alpha = \mu_n^+$ to be zero we find that

$$b_n^{(1)} = -\frac{(\delta/\beta)\sinh(\gamma(\mu_n^+))}{Q^+(\mu_n^+)\Delta'(\mu_n^+)\sinh(\gamma(\mu_n^+)a)}\left\{1+\sum_{m=0}^{\infty}\frac{a_m^{(1)}}{\mu_n^+-\alpha_m^+}\right\}. \tag{38}$$

We can now combine equations (37) and (38) to form a single algebraic equation, for $a_n^{(1)}$ say. Again, the first iterate of this equation was truncated to finite order, the truncated equation was solved numerically and the size of the truncation was increased until converged results were obtained. Numerical values for the $b_n^{(1)}$ can then be found from (38). In a similar way we eliminate the apparent poles in l_{21}^+ at $\alpha = \alpha_n^+$ and in l_{22}^+ at $\alpha = \mu_n^+$, to yield the pair of equations

$$\begin{aligned} a_n^{(2)} &= \epsilon_n Q^+(\alpha_n^+)\Delta(\alpha_n^+)(-1)^n \cos(n\pi a)/\alpha_n^+ \left[1 + \sum_{m=0}^{\infty} \frac{b_m^{(2)}}{\alpha_n^+ - \mu_m^+}\right] , \\ b_n^{(2)} &= -\frac{(\delta/\beta)\sinh(\gamma(\mu_n^+))}{Q^+(\mu_n^+)\Delta'(\mu_n^+)\sinh(\gamma(\mu_n^+)a)} \left\{\sum_{m=0}^{\infty} \frac{a_m^{(2)}}{\mu_n^+ - \alpha_m^+}\right\} , \end{aligned} \tag{39}$$

from which the unknowns $a_n^{(2)}$ and $b_n^{(2)}$ are found as above.

We have now constructed factors $\boldsymbol{\mathcal{L}}^{\pm}(\alpha)$ which are analytic in the respective half planes. However, as a final point, we need to check that these factors are also invertible. To do this we note that

$$\begin{aligned} \det\boldsymbol{\mathcal{L}}^-(\alpha) &= Q^-(\alpha)R(\alpha) , \\ \det\boldsymbol{\mathcal{L}}^+(\alpha) &= -\frac{R(\alpha)}{Q^+(\alpha)} , \end{aligned} \tag{40}$$

where

$$R(\alpha) = \left[1 + \sum_{m=0}^{\infty} \frac{a_m^{(1)}}{\alpha - \alpha_m^+}\right]\left[1 + \sum_{m=0}^{\infty} \frac{b_m^{(2)}}{\alpha - \alpha_m^+}\right] - \left[\sum_{m=0}^{\infty} \frac{a_m^{(2)}}{\alpha - \alpha_m^+}\right]\left[\sum_{m=0}^{\infty} \frac{b_m^{(1)}}{\alpha - \alpha_m^+}\right] . \tag{41}$$

Now, $R(\alpha)$ is an entire function of α, since the apparent poles at $\alpha = \alpha_m^+, \mu_m^+$ have been removed by the choice of the constants $a_m^{(1,2)}$ and $b_m^{(1,2)}$, and moreover it is observable that $R(\alpha) \to 1$ as $\alpha \to \infty$. Hence, by Liouville's Theorem $R(\alpha) \equiv 1$, and from (40) it follows that $\det\boldsymbol{\mathcal{L}}^{\pm}(\alpha)$ are nonzero in the upper/lower half planes, thanks to the corresponding properties of $Q^{\pm}(\alpha)$. This confirms that $\boldsymbol{\mathcal{L}}^{\pm}(\alpha)$ are invertible in their respective half planes.

We have now completed the factorisation of $\boldsymbol{\mathcal{L}}$, and have thereby determined all the previously unknown elements in the solution to our boundary value problem.

5. Results

We will be concerned with the acoustic far-field, and using the method of steepest descents it is straightforward to show that the pressure behaves as

$$p = \mathrm{i}\omega\rho\phi \sim \rho\frac{\mathcal{D}(\theta)}{\sqrt{r}}e^{\mathrm{i}\omega r} \quad \text{as } r \to \infty , \tag{42}$$

where ρ is the ambient fluid density and (r, θ) are polar coordinates centred on the origin. The pressure directivity $\mathcal{D}(\theta)$ is given by

$$\mathcal{D}(\theta) = \sqrt{\frac{\omega^3}{2\pi}} e^{\mathrm{i}\pi/4} D(\alpha_s) \sin\theta \ , \tag{43}$$

where $D(\alpha)$ is given in (18), and $\alpha_s = -\omega\cos\theta$ is the saddle point. The constants δ and β in (3) can be chosen freely in our solution, as long as the surface absorbs rather than releases energy (i.e. $\mathrm{Im}(\delta/\beta) \geq 0$), but for definiteness, and to relate our solution to other work on acoustic radiation for lined ducts in the aeroengine context, we introduce here the so-called wall impedance Z. Specifically, Z is defined to be the ratio between the wall pressure and the wall-normal velocity in the direction pointing into the wall, from which it follows that we can take $\delta = \mathrm{i}\omega$, $\beta = Z$. In contrast, the case of a rigid wall, $Z = \infty$, can be obtained setting by $\delta = 0$ in our solution. Alternatively, the rigid wall problem can be solved *ab initio*, in which case the kernel is now a 2×2 matrix which is factorised by one straightforward application of the pole removal technique (for brevity just the final result of this calculation is given in appendix C).

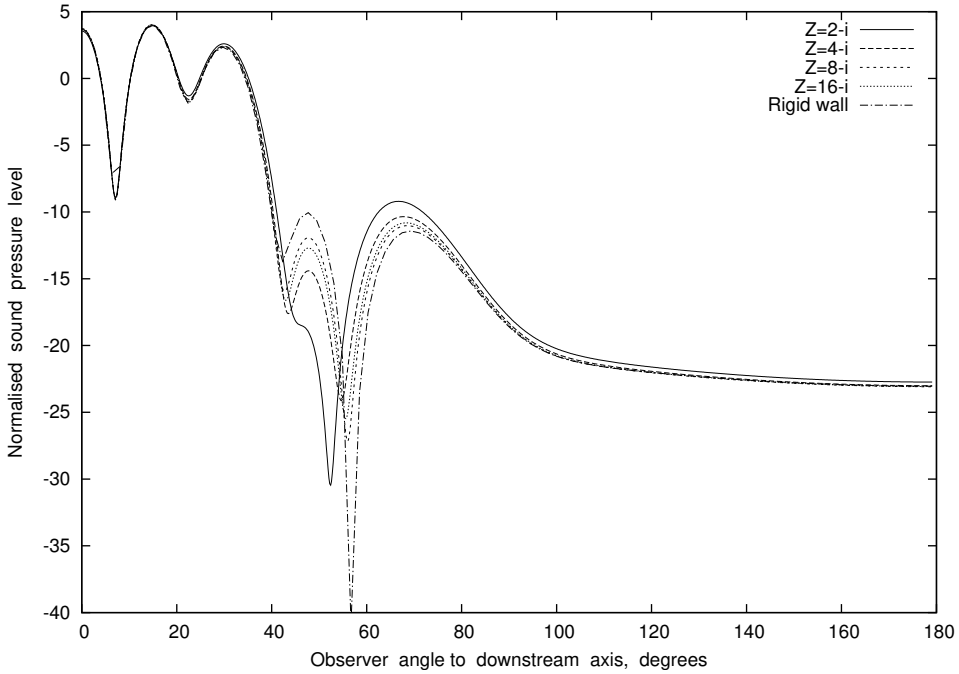

Figure 2: Normalised sound pressure level against observer angle to downstream axis. Here $\omega = 15$, $d = -1$, $a = 0.75$ and the incident wave is $\mu = \mu_0^-$, i.e. the least attenuated mode in the outer duct. The wall impedance Z takes a range of values.

In figures 2 & 3 we study the effect of varying Z on the normalised far-field sound pressure level (defined to be $20\log_{10}|\mathcal{D}(\theta)|$), with incident modes in the

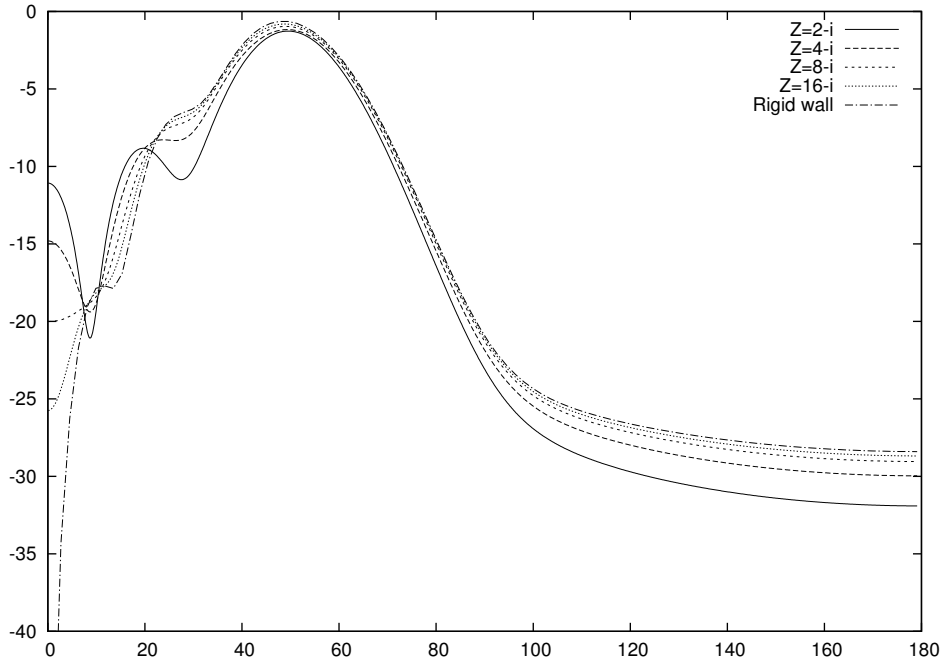

Figure 3: Normalised sound pressure level against observer angle to downstream axis. Here $\omega = 15$, $d = -1$, $a = 0.75$ and the incident wave is $\mu = \mu_1^-$, i.e. the second least attenuated mode in the outer duct. The wall impedance Z takes a range of values.

outer duct $\mu_{\rm inc} = \mu_0^-$ and $\mu_{\rm inc} = \mu_1^-$ respectively. Note that for finite values of Z the downstream[1] modes μ_n^- in the outer duct all decay with distance, and $\mu_{0,1}^-$ are the wavenumbers of the two least-decaying modes. In both cases it is clear that the value of Z has rather little effect in the directions of maximum radiation amplitude (θ small in figure 2 and $\theta \approx 50^\circ$ in figure 3). In the limit of large ω, Chapman [16] has shown that the modes propagating in a (cylindrical) duct can be described in terms of rays. In our two-dimensional problem the ray angles for modes in $d < x < 0$ are $\theta = \sin^{-1}(n\pi/\omega)$ for all n such that $n < \omega/\pi$. The amplitude of each mode present in $d < x < 0$ is determined by the complex scattering and rescattering of the incident wave by all the edges. However, if we think simply of the direct scattering of the incident mode by the edges $(d, \pm a)$ into downstream-going duct modes in $d < x < 0$, then as a rough guide it is well known that the most efficient scattering occurs into those modes whose ray angle most closely matches the incident wave angle. When downstream-going duct modes in $d < x < 0$ are scattered by the edges $(0, \pm 1)$, Chapman has also

[1]Here, and in what follows, we use the word 'downstream' to refer to the rightwards direction, in line with a key application of this model problem to the bypass and jet exhaust flows issuing from the rear of an aeroengine

shown (in the cylindrical case) that the contribution to the far-field directivity from each such duct mode is largest in the observer direction which matches the corresponding duct ray angle. In this way we can expect that the ray angle of the incident duct mode is imprinted on the far-field directivity, at least in the limit of large ω. If we take the ray angle (to the x axis) of the (evanescent) incident mode to be $\cos^{-1}[-\mathrm{Re}(\mu_{\mathrm{inc}}/\omega)]$, then it follows that the incident-mode ray angles in figures 2 & 3 for $Z = 2 - \mathrm{i}$ are approximately 14.98° and 62.61° respectively. The tilting of the dominant radiation direction from figure 2 to figure 3 is therefore consistent with the above argument. It is also clear from the results that the actual amplitude of the largest scattered field, as opposed to its direction, is rather insensitive to the value of Z.

It should also be noted that away from the principal radiation directions the field is highly dependent on Z. For instance, in figure 2, the field in the sideline direction is significantly modified, while in figure 3 it is the field in the downstream direction which changes most with Z (even changing from a local maximum to a near null as $|Z|$ increases). This is because the field in these directions is determined by the complicated interference between the radiation from all the scattered and multiply rescattered fields within the duct. The relative phasing of these components is then clearly sensitive to the precise value of Z, and this leads to the more major changes seen in the far field.

In figure 4 we hold Z fixed and vary d. We see that, as for variation of Z in figure 2, the radiation directly downstream is rather insensitive to d, but that more significant effects arise for larger values of θ, where one expects the interference between all the various scattered and multiply rescattered components to become important. In the case of a lossy liner one would expect that the field in $\theta > \pi/2$ would reduce as the inner duct is buried further and further upstream, and this is indeed borne out in figure 4.

We have already noted that our solution (18) is replaced by the very similar, but simpler, form (C.1) when the inner duct wall becomes rigid on both sides. If the inner duct wall is removed completely, so that one considers only the radiation from a single rigid duct $x < 0, y = \pm 1$, then it is easy to show via the scalar Wiener-Hopf technique that (18) is replaced by

$$D(\alpha) = \frac{e^{\gamma}}{\gamma} \left\{ \frac{q^{+}(\alpha) q^{-}(\mu_{\mathrm{inc}})}{\alpha - \mu_{\mathrm{inc}}} F \right\} , \tag{44}$$

where $q^{\pm}(\alpha)$ are given in (B.3), $F = K(-1)^N$ and N is the mode number of the incident mode. The structure of the answer is therefore maintained as the complexity of the model problem is increased, and it is interesting to note how the single-duct problem, as represented by the scalar function $q(\alpha)$, can still be seen in the more complicated solution presented in this paper. Moreover, the simplicity of (44) allows us to make a further comment about the results shown in this section. For $\theta \to \pi$, we see from (44) and (43) that the far-field directivity is proportional to

$$\frac{q^{+}(\omega)}{1 + \cos\chi} , \tag{45}$$

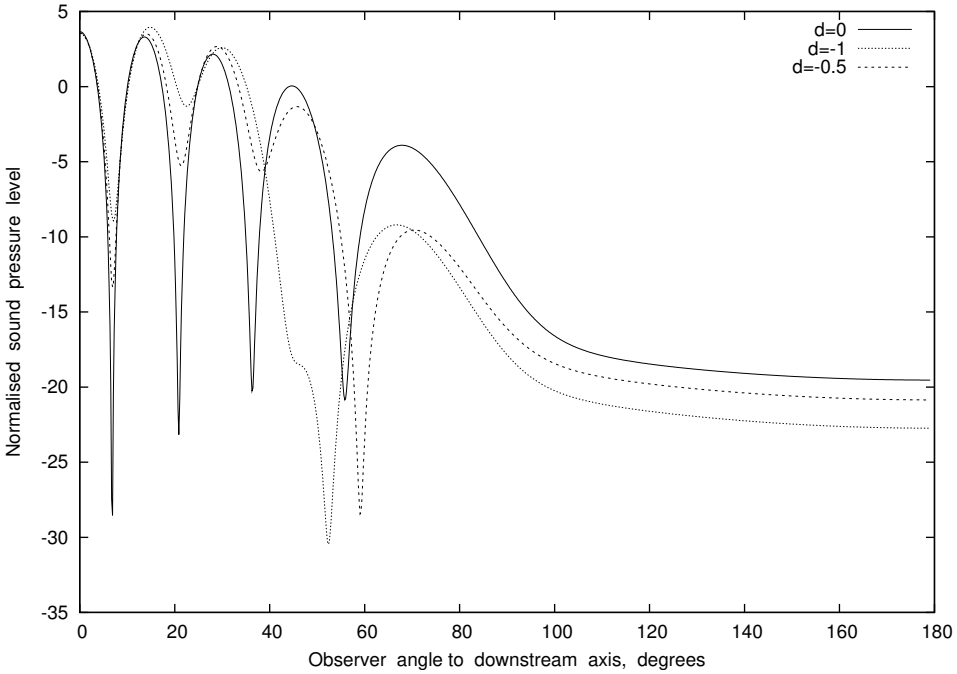

Figure 4: Normalised sound pressure level against observer angle to downstream axis. Here $\omega = 15$, $a = 0.75$, $Z = 2 - \mathrm{i}$ and the incident wave is $\mu = \mu_0^-$.The stagger d takes a range of values.

where $\chi = \sin^{-1} N\pi/\omega$ is the propagation angle of the incident mode in the single duct. Since ω is real and positive, and hence taken as a point in the upper half plane, it follows by construction that $q^+(\omega) \neq 0$. Therefore the sound radiated backwards is definitely nonzero (but of course is typically small). This point is clear in figures 2, 3 and 4. In the downstream direction, $\theta \to 0$, the far-field directivity is now proportional to

$$\frac{q^+(-\omega)}{1 - \cos\chi} \,, \tag{46}$$

and since $q(-\omega) = 0$ while $q^-(-\omega) \neq 0$ (as $-\omega$ lies in the lower half plane) it follows that for $\chi \neq 0$ the far-field sound must be exactly zero downstream for the simple single duct. The nonzero fields for $\theta = 0$ in figures 2, 3 and 4 must therefore be attributed to the scattering into the downstream-going plane-wave mode in $d < x < 0$.

All the results presented above are for an incident mode in the outer duct, so finally in figure 5 we consider instead an incident mode in the inner duct. As can be seen, the value of Z has very little effect on the radiated sound for almost all observer positions, apart from those close to the downstream axis. The fact that the effect of the lining is now so small is not surprising, since the incident field

in this case is no longer directly incident on the compliant surface. As noted in the previous paragraph, it is the plane-wave mode propagating downstream in the region $d < x < 0$, i.e. $\alpha = \alpha_0^-$, which radiates close to the downstream axis. The incident mode considered, $\kappa_{inc} = \kappa_2^-$, propagates with a significant transverse component, and in the rigid-wall case is very poorly coupled with the mode $\alpha = \alpha_0^-$ (which propagates purely in the axial direction). This is why the rigid-wall result in figure 5 attains a very low amplitude for $\theta \approx 0$, and the effect of finite Z is to increase the scattering of mode κ_2^- into mode α_0^-.

6. Concluding remarks

In this paper we have presented the solution for the radiation properties of a pair of semi-infinite, parallel-plate ducts in which the inner duct is buried inside the outer duct. When all the duct walls are rigid the resulting 2×2 Wiener-Hopf matrix can be factorised in a straightforward way using pole removal (see Appendix C). However, by allowing an impedance boundary condition to be applied on one of the internal walls we have shown here that we now have a 3×3 Wiener-Hopf matrix of a form which has not previously been considered in the literature and which is not directly amenable to standard techniques. The method presented in this paper therefore provides a new approach to a sub-class of matrix problems involving terms with exponential behaviour.

Further work on this problem is currently being completed in two directions. First, by replacing the parallel plates with circular cylinders (essentially just involving replacement of the hyperbolic functions in (14) with Bessel functions), and including mean flow effects. Second, by considering the case in which the inner duct protrudes beyond the outer duct termination. This second aspect is more difficult, since the unsteady flow around the protruding portion of the inner duct can no longer be expressed as a modal expansion, thereby removing the possibility of direct application of techniques based on pole removal. This issue could perhaps be approached using the techniques for the iterative solution of coupled integral equations developed by Abrahams & Wickham [17, 18, 19] for scattering by staggered plates, but instead some progress has been made using the alternative Padé approximant method first suggested by Abrahams [20, 21] and applied to rigid cylinders by Veitch & Peake [10]. Preliminary results in this direction were presented in [22].

References

[1] J.W.S. Rayleigh, The Theory of Sound, MacMillan, 1940.

[2] H. Levine, J. Schwinger, On the radiation of sound from an unflanged circular pipe, Physical Review 73 (1948) 383–406.

[3] G.F. Homicz, J.A. Lordi, A note on the radiative directivity patterns of duct acoustic modes, J. Sound Vib. 41 (3) (1975) 283–290.

[4] L.A. Weinstein, The Theory of Diffraction and the Factorization Method, Golem, 1969.

[5] R. Munt, The interaction of sound with a subsonic jet issuing from a semi-infinite cylinder, J. Fluid Mech. 83 (1977) 609–640.

[6] R. Munt, Acoustic transmission properties of a jet pipe with subsonic jet flow: I. the cold jet reflection coefficient., J. Sound Vib. 142 (3) (1990) 413–436.

[7] G. Gabard, R.J. Astley, Theoretical model for sound radiation from annular jet pipes: far- and near-field solutions, J. Fluid Mech. 549 (2006) 315–341.

[8] A.D. Rawlins, A bifurcated circular waveguide problem, IMA Journal of Applied Mathematics 54 (1) (1995) 59–81.

[9] B. Noble, Methods Based on the Wiener-Hopf Technique, Chelsea, 1988.

[10] B. Veitch, N. Peake, Acoustic propagation and scattering in the exhaust flow from coaxial cylinders, J. Fluid Mech. 613 (2008) 275–307.

[11] M.K. Myers, On the acoustic boundary condition in the presence of flow, J. Sound Vib. 71 (1980) 429–434.

[12] A. Rawlins, Radiation of sound from an unflanged rigid cylindrical duct with an acoustically absorbing internal surface, Proc. Roy. Soc. Lond. A 361 (1978) 65–91.

[13] A. Demir, S.W. Rienstra, Sound radiation from an annular duct with jet flow and a lined centerbody, in: 12'th AIAA/CEAS Aeroacoustics Conference, AIAA Paper 2006-2718, Cambridge, MA., USA, 2006.

[14] A. Demir, S.W. Rienstra, Sound radiation from a lined exhaust duct with lined afterbody., in: 16'th AIAA/CEAS Aeroacoustics Conference, AIAA Paper 2010-3947, Stockholm, Sweden, 2010.

[15] I.D. Abrahams, Scattering of sound by two parallel semi-infinite screens, Wave Motion 9 (1987) 289–300.

[16] C.J. Chapman, Sound radiation from a cylindrical duct. 1. ray structure of the duct modes and of the external field, J. Fluid Mech. 281 (1994) 293–311.

[17] I.D. Abrahams, G.R. Wickham, On the scattering of sound by two semi-infinite parallel staggered plates. I. explicit matrix Wiener-Hopf factorization, Proc. Roy. Soc. Lond. 420 (1988) 131–156.

[18] I.D. Abrahams, G.R. Wickham, The scattering of sound by two semi-infinite parallel staggered plates. II. evaluation of the velocity potential for an incident plane wave and an incident duct mode, Proc. Roy. Soc. Lond. 427 (1990) 139–171.

[19] I.D. Abrahams, G.R. Wickham, Genertal Wiener-Hopf factorization of matrix kernels with exponential phase factors, SIAM J. Appl. Math. 50 (1990) 819–838.

[20] I. Abrahams, On the solution of Wiener-Hopf problems involving noncommutative matrix kernel decompositions, SIAM J. Appl. Math. 57 (1997) 541–567.

[21] I. Abrahams, The application of Padé approximants to Wiener-Hopf factorization, IMA J. Appl. Math. 65 (2000) 257–281.

[22] N. Peake, B. Veitch, Models for acoustic propagation through turbofan exhaust flows - lined ducts, in: 15'th AIAA/CEAS Aeroacoustics Conference, no. 20093108 in AIAA Paper, Miami, Florida, 2009.

[23] S.W. Rienstra, N. Peake, Modal scattering at an impedance transition in a lined flow duct, in: 11'th AIAA/CEAS Aeroacoustics Conference, AIAA/CEAS Paper 2005-2852, Monterey CA, USA, 2005.

Appendix A. The factors of the 3×3 matrix $\boldsymbol{\mathcal{K}}(\alpha)$.

The factors of the 3×3 matrix $\boldsymbol{\mathcal{K}}(\alpha)$ have been found as follows:

$$k_{i1}^{+}(\alpha) = \frac{1}{q^{+}(\alpha)} \left\{ C_i + \sum_{n=0}^{\infty} \frac{q^{+}(\alpha_n^{+})}{\alpha - \alpha_n^{+}} e^{-\mathrm{i}\alpha_n^{+} d} \left[R_n^1 k_{i2}^{+}(\alpha_n^{+}) + R_n^2 k_{i3}^{+}(\alpha_n^{+}) \right] \right\}$$
$$- q^{+}(\alpha) e^{-\mathrm{i}\alpha d} \left(\left[\frac{\delta \cosh(\gamma a) + \beta\gamma \sinh(\gamma a)}{\gamma \sinh\gamma} \right] k_{i2}^{+}(\alpha) + \left[\frac{\sinh(\gamma a)}{\sinh\gamma} \right] k_{i3}^{+}(\alpha) \right) , \quad (A.1)$$

where the C_i are arbitrary constants which for definiteness we choose to be $C_1 = C_3 = 1, C_2 = -1$;

$$\begin{pmatrix} k_{i2}^{+}(\alpha) \\ k_{i3}^{+}(\alpha) \end{pmatrix} = [\boldsymbol{\mathcal{L}}^{+}(\alpha)]^{-1} \left\{ -\tilde{\boldsymbol{C}}_i + \sum_{m=0}^{\infty} e^{\mathrm{i}\alpha_m^{-} d} \frac{k_{i1}^{-}(\alpha_m^{-})}{\alpha - \alpha_m^{-}} \boldsymbol{\mathcal{L}}^{-}(\alpha_m^{-}) \begin{pmatrix} S_m^1 \\ S_m^2 \end{pmatrix} \right\} , \quad (A.2)$$

where the $\tilde{\boldsymbol{C}}_i$ are arbitrary constant vectors which for definiteness we choose to be $\tilde{\boldsymbol{C}}_1 = \tilde{\boldsymbol{C}}_2 = (1,1)^T$, $\tilde{\boldsymbol{C}}_3 = (1,-1)^T$;

$$k_{i1}^{-}(\alpha) = q^{-}(\alpha) \left\{ C_i + \sum_{n=0}^{\infty} \frac{q^{+}(\alpha_n^{+})}{\alpha - \alpha_n^{+}} e^{-\mathrm{i}\alpha_n^{+} d} \left[R_n^1 k_{i2}^{+}(\alpha_n^{+}) + R_n^2 k_{i3}^{+}(\alpha_n^{+}) \right] \right\} ; \quad (A.3)$$

and

$$\begin{pmatrix} k_{i2}^{-}(\alpha) \\ k_{i3}^{-}(\alpha) \end{pmatrix} = [\boldsymbol{\mathcal{L}}^{-}(\alpha)]^{-1} \left\{ \tilde{\boldsymbol{C}}_i - \sum_{m=0}^{\infty} e^{\mathrm{i}\alpha_m^{-} d} \frac{k_{il}^{-}(\alpha_m^{-})}{\alpha - \alpha_m^{-}} \boldsymbol{\mathcal{L}}^{-}(\alpha_m^{-}) \begin{pmatrix} S_m^1 \\ S_m^2 \end{pmatrix} \right\}$$
$$+ e^{\mathrm{i}d\alpha} k_{i1}^{-}(\alpha) \begin{pmatrix} -\sinh(\gamma a)/\sinh\gamma \\ \cosh(\gamma a)/\gamma \sinh\gamma \end{pmatrix} . \quad (A.4)$$

Appendix B. Multiplicative factorisation of $q(\alpha)$ and $Q(\alpha)$.

In this Appendix we present the multiplicative factorisation of the two scalar functions

$$q(\alpha) \equiv \gamma e^{-\gamma} \sinh\gamma \tag{B.1}$$

and

$$Q(\alpha) = \frac{\sinh\gamma}{\Delta \sinh(\gamma a)} \tag{B.2}$$

given in (22) and (33) respectively.

First, we define $\tilde{q}(\alpha) = 2q(\alpha)/\gamma$, which has the property that $\tilde{q} \to 1$ as $\alpha \to \pm\infty$ along the real line. The multiplicative factorisation of $\tilde{q}(\alpha)$ can then be completed using Cauchy integrals, to leave us with

$$q^{\pm}(\alpha) = \frac{\gamma^{\pm}(\alpha)}{\sqrt{2}} \exp\left[\pm\frac{1}{2\pi \mathrm{i}} \int_C \frac{\log\tilde{q}(\xi)}{\xi - \alpha} \mathrm{d}\xi\right] , \tag{B.3}$$

where $\gamma^{\pm}(\alpha) = e^{\pm \mathrm{i}\pi/4}(\alpha \pm \omega)^{1/2}$ are the usual multiplicative factors of $\gamma(\alpha)$ (see e.g. Noble [9]). The contour C is the real axis deformed to lie above/below all poles and zeros of q (and Q) lying in the lower/upper half plane, and we have used the parametric form for C proposed by Rienstra [23],

$$\xi = t - \frac{4\mathrm{i}\mathfrak{D}(t/\mathfrak{W})}{3 + (t/\mathfrak{W})^4} , \tag{B.4}$$

where $-\infty < t < \infty$. The width and height parameters $\mathfrak{W}$ and $\mathfrak{D}$ are chosen to ensure that C lies above/below all modes in the lower/upper half planes. The integral in (B.3) can easily be computed numerically by mapping onto the finite interval $-1 < s < 1$ using the transformation $t = s/(1-s^2)^2$, and standard quadrature routines can then be employed to evaluate the finite integral numerically. We observe from (B.3) that $q^{\pm}(\alpha) \sim e^{\pm \mathrm{i}\pi/4}\sqrt{\alpha/2}$ as $\alpha \to \infty$ in the upper/lower half planes.

The multiplicative factorisation of $Q(\alpha)$ is completed by introducing $\tilde{Q}(\alpha) = -\beta\gamma Q(\alpha)/2$, which is such that $\tilde{Q} \to 1$ as $\alpha \to \infty$. It then follows that

$$Q^{\pm}(\alpha) = \frac{\mathrm{i}\sqrt{2/\beta}}{\gamma^{\pm}(\alpha)} \exp\left[\pm\frac{1}{2\pi \mathrm{i}} \int_C \frac{\log\tilde{Q}(\xi)}{\xi - \alpha} \mathrm{d}\xi\right] . \tag{B.5}$$

We observe from (B.5) that $Q^{\pm}(\alpha) \sim \mathrm{i}e^{\pm \mathrm{i}\pi/4}\sqrt{2/(\beta\alpha)}$ as $\alpha \to \infty$ in the upper/lower half planes.

One important aspect of the calculation of (B.3,B.5) is the need to monitor $\tilde{q}(\xi)$ and $\tilde{Q}(\xi)$ along the contour C to ensure that their arguments do not vary by more than 2π.If this were to happen then the logarithm would approach some multiple of $2\pi\mathrm{i}$ at infinity, the integral would no longer converge and the sort of treatment described in Appendix A of [10] based on example 1.12, page 42 of [9] would be required. However, this has been monitored carefully in our calculations, and we have found no examples of the logarithmic branch cut being crossed for the parameter values considered.

In Figure 6 we plot C, the branch cuts which define γ and the lowest values of $\alpha_n^{\pm}$ and $\mu_n^{\pm}$ in a typical case.

Appendix C. Solution for rigid walls.

In this appendix we state the solution for the case in which all the walls are rigid (i.e. $\delta = 0$ and, without loss of generality, $\beta = 1$). In parallel with equation (18), the unknown coefficient in the solution for $y > 1$ is given by

$$D(\alpha) = \frac{e^{\gamma}}{\gamma}\left\{\frac{[\tilde{\boldsymbol{\mathcal{K}}}^{+}(\alpha)]^{-1}\tilde{\boldsymbol{\mathcal{K}}}^{-}(\mu_{\rm inc})\tilde{\boldsymbol{F}}}{\alpha-\mu_{\rm inc}} + \frac{[\tilde{\boldsymbol{\mathcal{K}}}^{+}(\alpha)]^{-1}\tilde{\boldsymbol{\mathcal{K}}}^{-}(\kappa_{\rm inc})\tilde{\boldsymbol{G}}}{\alpha-\kappa_{\rm inc}}\right\}_1 . \qquad \text{(C.1)}$$

Here the 3×3 matrix $\boldsymbol{\mathcal{K}}$ has been replaced by the 2×2 matrix $\tilde{\boldsymbol{\mathcal{K}}}$, given by

$$\tilde{\boldsymbol{\mathcal{K}}} = \frac{1}{\Delta}\begin{pmatrix} -e^{(1-a)\gamma} & e^{{\rm i}\alpha d} \\ -e^{-{\rm i}\alpha d} & \frac{\sinh\gamma}{\sinh(\gamma a)} \end{pmatrix} , \qquad \text{(C.2)}$$

with

$$\Delta = -\gamma\sinh\gamma(1-a) , \qquad \text{(C.3)}$$

and the vectors $\tilde{\boldsymbol{F}}, \tilde{\boldsymbol{G}}$ have components equal to the first two components of $\boldsymbol{F}, \boldsymbol{G}$. Again, the factorisation of $\tilde{\boldsymbol{\mathcal{K}}}^{+}(\alpha)$ in the form $\tilde{\boldsymbol{\mathcal{K}}}^{-}\tilde{\boldsymbol{\mathcal{K}}} = \tilde{\boldsymbol{\mathcal{K}}}^{+}$ is required, and is completed via a straightforward application of the pole-removal technique. The elements in the factors $\tilde{\boldsymbol{\mathcal{K}}}^{\pm}(\alpha)$ are found to be:

$$\tilde{k}^{+}_{i1}(\alpha) = \frac{C_i}{q^{+}(\alpha)} - e^{-{\rm i}\alpha d}\frac{\sinh(\gamma a)}{\sinh\gamma}\tilde{k}^{+}_{i2}(\alpha) + \sum_{n=1}^{\infty}\frac{e^{-{\rm i}\alpha^{+}_n d}R^{+}_n q^{+}(\alpha^{+}_n)\tilde{k}^{+}_{i2}(\alpha^{+}_n)}{q^{+}(\alpha)(\alpha-\alpha^{+}_n)} , \qquad \text{(C.4)}$$

where for definiteness we take $C_1 = 1$, $C_2 = -1$;

$$\tilde{k}^{+}_{i2}(\alpha) = Q^{+}(\alpha)\left\{D_i + \sum_{m=1}^{\infty}\frac{e^{{\rm i}\alpha^{-}_m d}R^{-}_m Q^{-}(\alpha^{-}_m)\tilde{k}^{-}_{i1}(\alpha^{-}_m)}{(\alpha-\alpha^{-}_m)}\right\} , \qquad \text{(C.5)}$$

where for definiteness we take $D_1 = D_2 = 1$;

$$\tilde{k}^{-}_{i1}(\alpha) = q^{-}(\alpha)\left\{C_i + \sum_{n=1}^{\infty}\frac{e^{-{\rm i}\alpha^{+}_n d}R^{+}_n q^{+}(\alpha^{+}_n)\tilde{k}^{+}_{i2}(\alpha^{+}_n)}{(\alpha-\alpha^{+}_n)}\right\} ; \qquad \text{(C.6)}$$

and

$$\tilde{k}^{-}_{i2}(\alpha) = \frac{D_i}{Q^{-}(\alpha)} - e^{{\rm i}\alpha d}\frac{\sinh(\gamma a)}{\sinh\gamma}\tilde{k}^{-}_{i1}(\alpha) + \sum_{m=1}^{\infty}\frac{e^{{\rm i}\alpha^{-}_m d}R^{-}_m Q^{-}(\alpha^{-}_m)\tilde{k}^{-}_{i1}(\alpha^{-}_m)}{Q^{-}(\alpha)(\alpha-\alpha^{-}_m)} . \qquad \text{(C.7)}$$

Here, as before, $q(\alpha)$ and $Q(\alpha)$ are given by (22) and (33) respectively, with the modified definition definition of Δ given in (C.3), and $R^{\pm}_n = -n\pi(-1)^n\sin(n\pi a)/\alpha^{\pm}_n$. The unknown values $\tilde{k}^{-}_{i1}(\alpha^{-}_n)$ and $\tilde{k}^{+}_{i2}(\alpha^{+}_n)$ can be determined by setting $\alpha = \alpha^{-}_m$ in (C.6) and substituting into (C.5) to yield an infinite system of linear equations. These are then truncated to finite order and solved numerically.

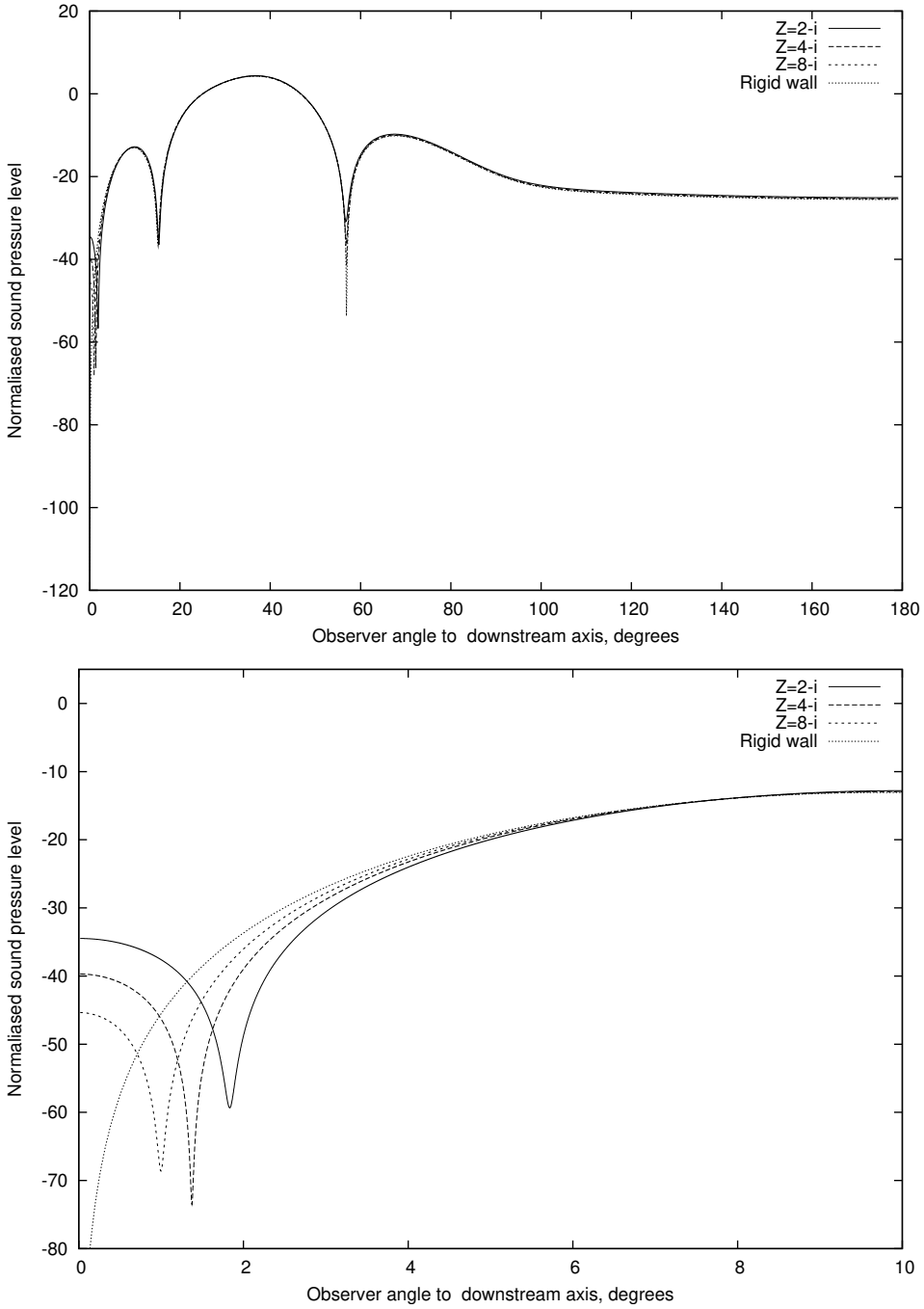

Figure 5: Normalised sound pressure level against observer angle to downstream axis, with magnified view for small observer angle. Here $\omega = 15$, $a = 0.75$, $d = -0.5$ and Z takes various values. The incident wave is $\mu = \kappa_2^-$, i.e. the third cut-on mode in the inner duct.

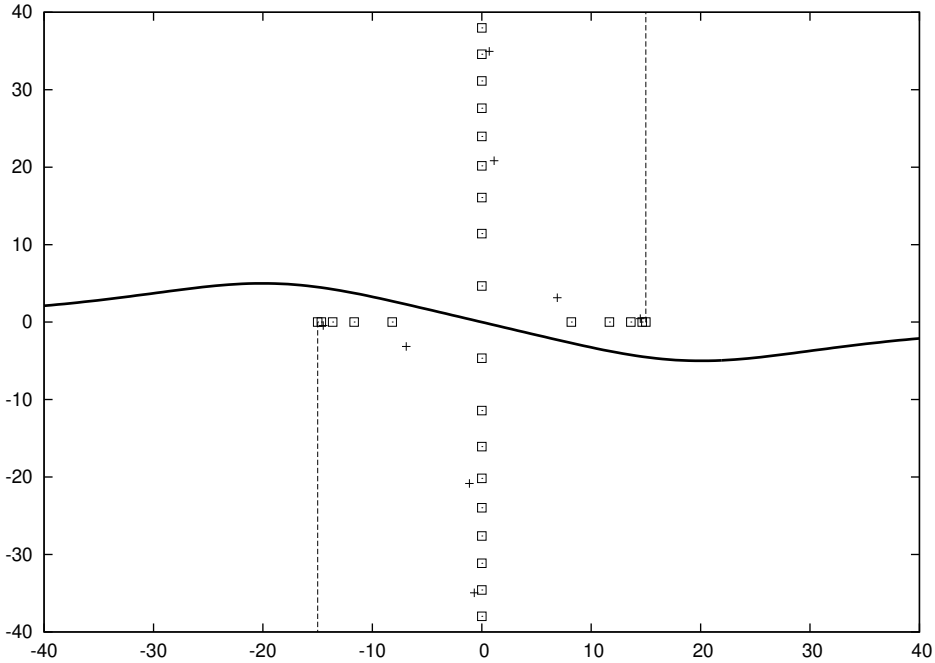

Figure 6: Sample plot of the complex α plane, showing the integration contour C (solid line), branch cuts (dashed lines) and various modal wavenumbers involved in the factorisation - $\alpha_n^{\pm}$ (square symbols) and $\mu_n^{\pm}$ (plus symbols). Here $\omega = 15$, $a = 0.75$ and $Z = 2 - \mathrm{i}$.